www.cadanda.com
Computer-Aided Design AND APPLICATIONS

Automatic Feature Identification in Dental Meshes

Yokesh Kumar[1], Ravi Janardan[1] and Brent Larson[2]

[1]University of Minnesota, {kumaryo, janardan}@cs.umn.edu
[2]Division of Orthodontics, University of Minnesota, larso121@umn.edu

ABSTRACT

The goal of virtual orthodontic treatment planning is to re-position the teeth in a digital dental model so that the desired alignment of the teeth on each dental arch and occlusion (i.e., matching) of the upper and lower arches is achieved. The input to the planning process is a collection of individual tooth objects obtained by segmenting a noisy 3D surface mesh that is generated by laser-scanning a plaster model of the dental arch built from patient-specific dental impressions. A key step in the planning is the identification of features on the surface of the teeth such as cusps, grooves, incisal edges, marginal ridges, and occlusal surface boundary, that are important both for carrying out the alignment and evaluating its quality. This paper presents a collection of techniques to identify such features automatically, with minimal user intervention. Experimental results are presented that show the effectiveness of the approach.

Keywords: tooth segmentation, feature identification, digital orthodontics.
DOI: 10.3722/cadaps.2012.747-769

1 INTRODUCTION

Orthodontic treatment planning seeks to re-position the teeth in the dental arches of a patient in order to achieve an outcome that is both aesthetically pleasing and functionally optimal. Technological advances now make it possible for the treatment plan to be simulated virtually (in 3D) and allow the clinician to choose between multiple alternatives in order to achieve the best possible outcome. Virtual planning begins with the acquisition of a 3D surface mesh of each arch. This mesh is generated by building a plaster model of each arch from patient-specific dental impressions and then laser-scanning the model. The mesh is then segmented into individual tooth objects (i.e., submeshes), using, for instance, the algorithms in [11, 12]. These tooth objects are the input to the alignment process, which involves proper repositioning of teeth relative to one another in each arch and proper matching of the contact regions between teeth in different arches.

1.1 Dental Features and their Importance

Proper orthodontic tooth alignment and functionality (e.g., chewing) depend on a number of intrinsic features on the tooth surface, including cusps, grooves, incisal edges, ridges, occlusal contact region, etc. (These terms are defined in Section 2.) These features are important for many reasons: They provide a set of landmarks that can be used to define alignment requirements quantitatively (e.g., height difference between adjacent marginal ridges) [18]. Also, the features themselves do not change over time (as they are intrinsic to the tooth surface), so they can be used to monitor the progress of the alignment. Moreover, since certain (derived) features need to remain invariant throughout treatment (e.g., the distance between canine tips), the intrinsic features dictate the best possible alignment that can be achieved and provide a means for evaluating a computed alignment. Finally, features such as number of cusps are useful in classifying teeth automatically (e.g., molars, premolars, etc.).

Dental features have applications in other related areas. In the field of computer-aided planning and simulation in craniomaxillofacial surgery, the correct dental occlusion or the *maximum intercuspation* of digital 3D representations of the arches of a patient must be reestablished. This is in general difficult in a virtual environment and is approximately computed by aligning the grooves and marginal ridges of the upper arch with the corresponding cusps and incisal edges of the lower arch [4]. Also, finer dental occlusion depends on getting a close fit in the areas of contact between the surface of the two arches [4, 8]. It is known that only the tooth surface regions bounded by the occlusal and marginal ridges participate in occlusal contacts. Thus, these features can significantly speed up the surface matching and alignment algorithms in virtual surgical planning.

1.2 Goals and Contributions

The identification of a relevant feature set is crucial for orthodontic treatment planning. However, identifying features manually, by having a clinician **ò**eyeball**ó** each tooth is labor-intensive, time-consuming, and prone to error. Our goal is to identify intrinsic tooth surface features (cusps, ridges, grooves, etc.) automatically, with intervention by the clinician to verify or correct identified features only in difficult or unusual cases. In this paper, we discuss the computational issues associated with automatic feature identification and present a collection of algorithms to do this effectively. Our algorithms are based on curvature analysis, clustering on 2D cross-sections of tooth surfaces, and an adaptation of the watershed method for segmentation. We have incorporated our algorithms in a software tool and we present experimental results that show that our methods are effective at automatic feature identification on noisy and incomplete real-world datasets.

1.3 Challenges in Feature Identification

The input to the feature identification task is a collection of meshes representing individual tooth objects (Figure 1). The feature identification task is complicated by the fact that the meshes are almost always noisy and incomplete. This is due to the limitations (resolution) of the laser scanning process itself in the presence of malocclusions and crowding of teeth, as well as variations across different types of scanners. A practical requirement of the feature identification algorithms that we seek is that they should be robust to noise and missing information.

1.4 Organization of the Paper

Section 2 defines relevant anatomical terms and the features of interest. Section 3 describes an algorithm for cusp identification based on the familiar watershed method. Section 4 introduces a general approach based on curvature analysis and clustering on 2D cross-sections of tooth surfaces for identifying other features such as incisal edges, grooves, marginal ridges, and occlusal surface boundary. Section 5 discusses how these features are identified and presents the results on some

cases. Section 6 describes the identification of some derived features and Section 7 discuss the evaluation of the developed techniques on real-world clinical data. Section 8 offers concluding remarks.

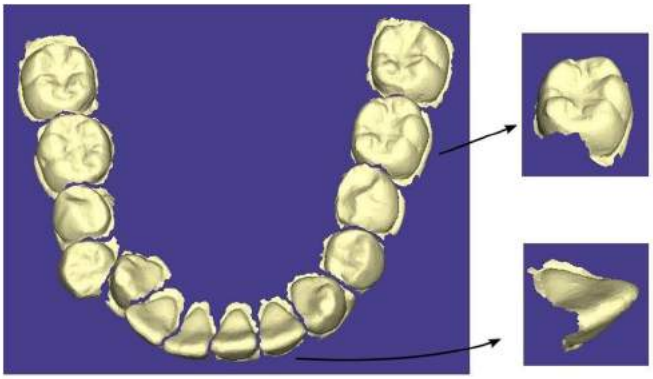

Fig. 1: Input to the feature identification task. A segmented lower arch is shown on the left and the individual meshes, representing tooth objects, are shown on the right. One can note the highly irregular occlusal surfaces of molars and premolars that tend to create problems for the detection of ridges, grooves and cusps.

2 DENTAL ANATOMY AND DENTAL FEATURES

2.1 Dental Anatomy

Teeth are classified as *incisors*, *canines*, *premolars* and *molars*. Each *dental arch*, i.e., row of teeth, can be divided into a *left* and a *right* side. Each side has two incisors (*central* and *lateral*), one canine, two premolars (*first* and *second*) and three molars (*first*, *second* and *third*). The incisors and canines are collectively called *anteriors* and are used in cutting action. The premolars and molars are called *posteriors* and are involved in chewing action.

The inner (resp. outer) part of the tooth on the tongue (resp. face) side is called the *lingual* (resp. *facial*) side. The face side on posteriors (resp. anteriors) is called the *buccal* (resp. *labial*) side. A tooth's surface towards the front (resp. back) of the arch, i.e., towards (resp. away from) the central incisors, is called the *mesial* (resp. *distal*) side.

A suitably chosen line through the mesial and distal side of each tooth defines the *mesiodistal* line of the tooth. Similarly, the lingual and buccal (or labial) sides define the *buccolingual* line. These lines are important in feature identification and in understanding tooth functionality. All definitions above are illustrated in Figure 2.

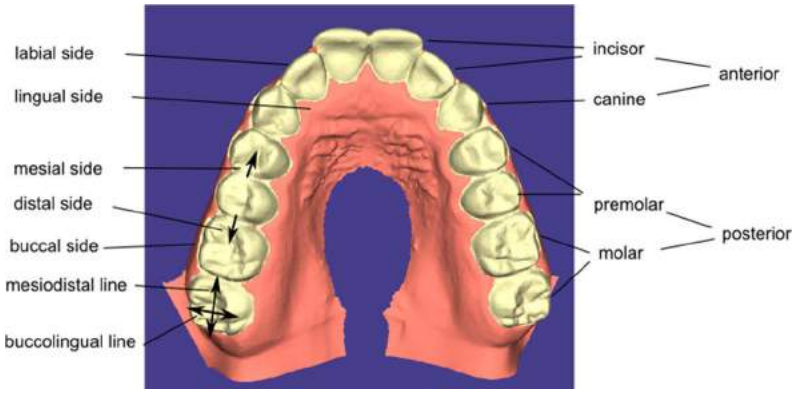

Fig. 2: Dental anatomy.

2.2 Dental Features

Now, we define some of the features on tooth surfaces that are important in orthodontic treatment planning. The surface of the teeth resembles a terrain with **ò**mountain peaks", **ò**ridges" and **ò**valleys". For the ease of understanding, it is convenient to define dental features in terms of these terrain-like features. More details on dental anatomical features can be found in textbooks such as [23].

Incisal edges: These are the sharp ridges on the anteriors (incisors and canines) running along the mesiodistal line. Figure 3 shows an example.

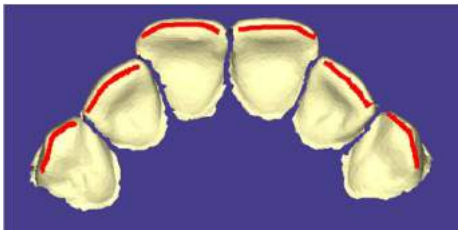

Fig. 3: Incisal edges on the anterior teeth (shown as red curves).

Cusps: On premolars and molars these are the mountain peak-like structures on the surface, at the corners of the tooth. Each cusp has *cusp ridges* radiating from its tip, similar to ridges that connect mountain peaks to valleys on a terrain; these can be used to define other features such as the occlusal surface boundary (explained below).

Canines have a single cusp which plays an important role in determining the overall quality of the alignment. The premolars (resp. molars) have 2 or 3 (resp. 4 or 5) cusps depending on the arch (upper or lower) and the individual. These cusps are named according to their position on the tooth surface. For example, a molar would have a mesiolingual cusp situated on the mesial and lingual side of the tooth. Similarly, for mesiobuccal, distolingual, distobuccal, lingual and buccal cusps. Some of these cusps are shown in Figures 4 and 5.

Occlusal surface and marginal ridges: The *occlusal surface* of a posterior tooth is the area of the tooth surface where chewing occurs. This is also the contact area between corresponding posterior teeth from opposing arches (Figure 4). Thus, the occlusal surface complements the functionality of incisal edges.

The *marginal ridges* are located at the mesial and distal ends of the occlusal surface. These are the regions where the mesial or distal walls of a tooth make contact with the occlusal surface (Figure 4). Thus, each tooth has a mesial and a distal marginal ridge. For incisors, the marginal ridges are on the vertical sides of the teeth since the occlusal surface of incisors is the lingual (resp. labial) surface on the upper (resp. lower) arch.

The occlusal surface of a posterior tooth is bounded on the buccal and lingual sides by the cusp ridges (inclusive of the cusps). On the mesial and distal sides, the occlusal surface is bounded by the two marginal ridges. This provides a boundary around the occlusal surface area called *occlusal surface boundary* (Figure 4). Thus, the occlusal surface boundary is a curve on the tooth surface that connects the marginal ridges, cusp ridges, and the cusp peaks.

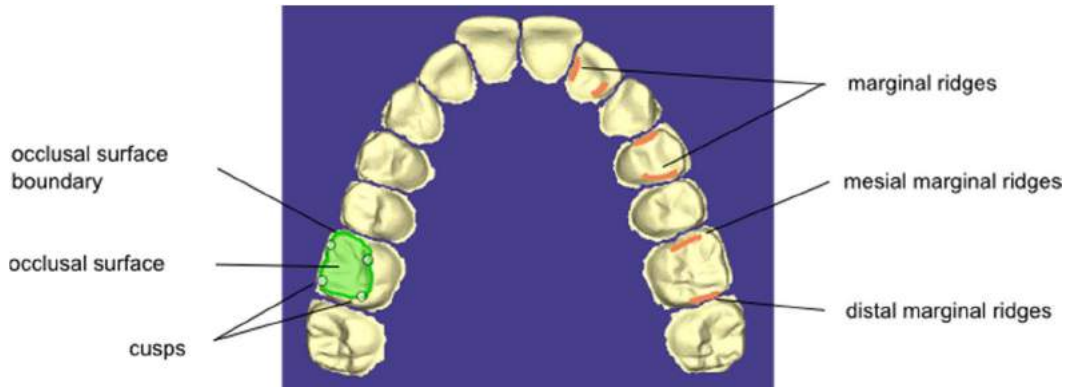

Fig. 4: Cusps, marginal ridges, and occlusal surface boundary in an upper arch, as found by our feature identification algorithms. Note the difference in the marginal ridges on incisors and posteriors.

Grooves: These are the depressions and fissures on the occlusal surface of a posterior tooth that resemble riverbeds and valleys on a terrain. There are various types of grooves and corresponding classification and naming conventions. For our study, we are interested in the long grooves running along the mesiodistal line of the tooth, called *central developmental grooves*, or just *central grooves*. Figure 5 shows some examples of (approximations of) grooves that are useful for orthodontic purposes.

Figure 5 also highlights the difference between the grooves on the premolars on the upper and lower arch (these are more curved). On the other hand, the grooves on lower arch molars are much more straight than their upper arch counterparts. Additional groove types and their uses can be found in [23].

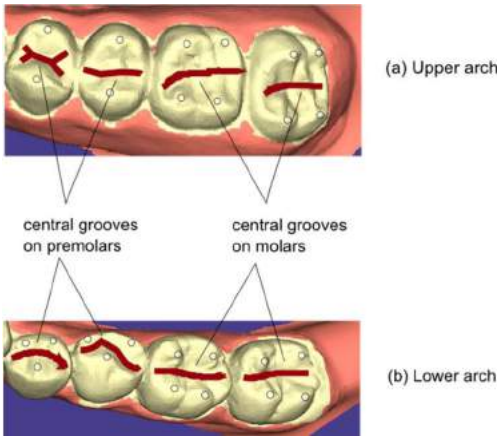

Fig. 5: Grooves on the molars and premolars of the lower and upper arch. Many different types of grooves can be defined on the tooth surface based on their position and dimensions. The images above show the approximation of the central grooves that are believed to be the most relevant for orthodontic treatment planning. The circles indicate the cusps on teeth.

Other derived features: In addition to the above-mentioned features, which are intrinsic to the tooth surface, there are other features that are derived from these intrinsic features and are important in alignment. These include the archform and the occlusal plane [23].

The *archform* is defined as an appropriate smooth curve through the incisal edges of anteriors, canine cusps and the buccal cusps of molars and premolars (Figure 6). The archform determines the overall quality achievable by the alignment process.

The *occlusal plane* is defined as a smooth surface passing through the occlusal or biting surfaces of the teeth. It is an imaginary surface at which the upper and lower arches meet and is important in establishing the vertical positioning and the buccolingual orientation of teeth in the final alignment.

Fig. 6: Archform of a dental model.

3 CUSP IDENTIFICATION

This section describes the identification of cusps on tooth surfaces. Our approach is based on the watershed class of algorithms [15] for mesh segmentation, reviewed briefly in Section 3.1.

3.1 Watershed-based Mesh Segmentation

This is a class of mesh segmentation algorithms that partition the mesh using the analogy of flooding of the mesh [15]. As an illustration, consider the one-dimensional curve shown in Figure 7. Each point on the curve is assigned a real-valued height using a height function $H : v(x, y) \rightarrow R$. In Figure 7, the height is simply the point's vertical elevation from the base (i.e., its y-coordinate). Imagine that each point on this curve has a drop of water stored as initialization. During the course of the algorithm, the water drop flows towards its most steep neighbor (with respect to the height function) until it reaches a minima point. The initial positions of the water drops are shown as the filled circles in Figure 7 along with the direction of their flow. The water is thus collected in catchment basins which are defined by a single local minimum point shown as an empty circle at the bottom of the curve. All the points that are visited by a water drop during its flow to a minimum point are given the same label, which is denoted by the minimum point. This process partitions the curve into regions defined by the labels as shown in Figure 7. In the vicinity of a flat (i.e., zero-slope) portion of the curve, we can choose to arbitrarily advance the flow in either direction so that a valid partitioning is achieved.

This technique was generalized to segmentation of 3D surfaces by Mangan and Whitaker [15] who used the surface curvature value for the height function. The algorithm in the form described is cumbersome to implement because we have to keep track of each flow and also use placeholders for assigning labels to vertices on its path because the final local minima of the flows are not known beforehand. Many improved implementation schemes have been suggested in the literature to overcome these difficulties [19].

These algorithms do not compare well with negative minima-based approaches for mesh segmentation as they are not very good at finding partition boundaries in arbitrary meshes (see [19, 20] for details). However, they are good at finding the different local minima of a given height function, but often lead to over-segmentation (i.e., a large number of partitions). Thus, to obtain large meaningful partitions, it is often necessary to merge small-sized spurious partitions with other partitions in their neighborhood. For example, Figure 7 shows a set of three initial partitions resulting from the procedure described above. However, if the goal is to find less than three partitions, we may merge partitions 1 and 2 instead of partitions 2 and 3 (depending on the *depth*, i.e., the smallest height difference between the minimum of a partition and any boundary point of that partition) to reduce the number of final partitions.

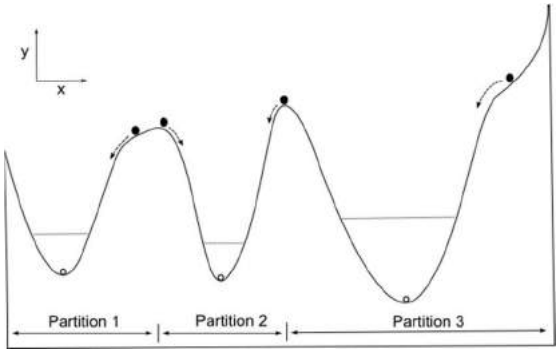

Fig. 7: Example illustrating the watershed-based approach to segmentation.

3.2 Watershed-based Cusp Detection

As mentioned in Section 3.1, watershed-based techniques are well-suited to find the cusps on the tooth surface which are defined as vertices corresponding to local minima for some intuitively defined height function. (For teeth on the upper arch, cusps are local minima while for those on the lower arch they are local maxima; we treat both cases uniformly, as local minima, by negating vertex coordinates in the latter case.)

The key to watershed-based cusp extraction is designing a good height function H. Most generic mesh segmentation schemes define H solely on the basis of surface curvature, so as to be able to segment meshes from a variety of sources. Here we take advantage of the fact that we are dealing with tooth surfaces and we define H on the basis of both surface curvature and the elevation of the vertices (i.e., their z-coordinates, since the scanned meshes are provided with a base that is parallel to the xy-plane). More precisely, for a vertex v on the surface of a tooth in the upper arch, we define its height as $H_v = (1-\alpha)\cdot(-K_v) + \alpha \cdot v_z$, where v_z is $v$ís z-coordinate, K_v is the surface curvature at v [16], and α is a parameter that controls the relative influence of K_v and v_z on H_v. In our implementation, we found that choosing α from the interval $[0.4, 0.6]$ worked well for all the models tested.

3.3 Results and Discussion

Figure 8 shows the result of applying the cusp identification algorithm with the above height function on three different models. Figure 8(a) shows a lower arch in which teeth are not well-aligned. Figures 8(b) and 8(c) show two upper arches where the molars are rotated away from the vertical z-axis by different amounts. Note that the number of cusps for teeth on the lower arch can be four or five, and we may sometimes have to deal with partially erupted molars.

(a) (b) (c)

Fig. 8: Cusps (shown red) identified using watershed method.

After the cusps have been identified automatically, our software tool allows the user to fine-tune the results manually (for very difficult cases) by clicking on the tooth surface to add/delete (hence move) cusps. For instance, a click to add a cusp triggers a search for the local minimum in a small neighborhood of the surface around the location of the click and places a cusp at this minimum. Thus the user does not have to ìeyeballî the mesh to find the exact location of the desired cusp.

4 A GENERAL APPROACH TO FEATURE IDENTIFICATION

In this section we discuss how to identify the remaining features of interest (beyond cusps), i.e., incisal edges, central grooves, marginal ridges, and occlusal surface boundary. It turns out that these features can all be identified using a general approach that is based on computing certain 2D cross-sections of the tooth surface, analyzing the curvatures of the (piecewise-linear) curves that define these cross-

sections to determine points of sufficiently high (positive or negative) curvature, and identifying clusters of such points that form the features of interest.

Our approach starts by creating a sequence of parallel planar cross-sections of the tooth surface, one set oriented along the mesiodistal line and one along the buccolingual line. For each cross-section in each set, we perform 2D curvature analysis at the vertices of the piecewise-linear curve that defines the cross-section and identify points of high curvature and cluster these to identify regions of interest on each curve. Then appropriate regions are selected from each curve and stitched together with those from curves of neighboring parallel cross-sections to obtain a connected and coherent feature (e.g., a ridge or groove). Thus, this approach provides a means to extract the desired 3D features in a **ò**guided**ó** fashion from a set of 2D regions of interest on individual cross-sections. This has several advantages over an approach that attempts to extract features directly, via curvature analysis in 3D, as we will discuss in Section 4.5. We will now explain the main steps of the approach in detail.

4.1 Computing a Medial Curve

Consider the left side of the arch in Figure 2. We can define a curve that passes suitably through the mesial and distal sides of each tooth on the left side starting from the last molar and ending at the central incisor. A similar curve can be defined for the right side of the arch. These two curves meet at the mesial sides of the two central incisors. We define the *medial curve* of the arch as the curve obtained by joining the curves from the left and right sides of the arch. (The term **ò**medial curve**ó** signifies that the curve involves both the mesial and distal sides of each tooth on the arch.) The medial curve will guide the feature identification process outlined above. The medial curve represents an approximate layout of all the teeth on the arch and also provides a mesiodistal line for each tooth that will be needed to compute the mesiodistal cross-sections, as we will see in Section 4.2.

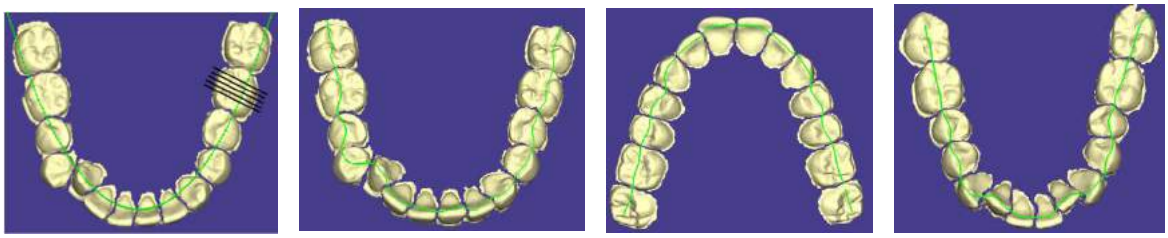

(a) (b) (c) (d)

Fig. 9: Computation of a medial curve (shown green): (a) Initial fit of the arch with a cubic curve. (b) Computed medial curve for arch in (a). Additional examples of medial curves on an upper arch (c) and a lower arch (d).

The medial curve is not unique since many different curves can satisfy the given definition. For our purposes, it suffices to have an approximate medial curve that reliably identifies the mesial, distal, buccal (labial) and lingual sides of a tooth. Accordingly, we compute the medial curve as shown below. Figure 9 shows the results of this algorithm.

Computing medial curve of an arch

1. Project the triangular faces on each tooth surface to a set of triangles, F_{xy}, on the xy-plane.
2. Find a cubic curve C_{fit} that best fits the 2D projections of the vertices in F_{xy} (Figure 9(a)).

3. Sample the length of C_{fit} at suitably small intervals to get an ordered sequence, $P = p_1, p_2, \ldots, p_n$ of points on C_{fit}.
4. At each point $p_i \in P$, define a line l_i orthogonal to C_{fit} (Figure 9(a)). Find the median point, m_i, of the intersection points of l_i with F_{xy}. Output the medial curve as the piecewise-linear curve that connects the ordered sequence, $C_{med} = m_1, m_2, \ldots, m_n$ of medians (Figure 9(b)).

4.2 Computing Planar Cross-Sections

Using the medial curve described above, we compute an approximation, L_{md} of the mesiodistal line, of a given tooth by finding the best-fitting line segment for the section of the medial curve segment that goes through the tooth. We can also compute an approximation, L_{bl}, of the buccolingual line of the tooth by taking the line orthogonal to the mesiodistal line and passing through the centroid of the *xy*-projection of the tooth. We will refer to the approximation of the mesiodistal (resp. buccolingual) line as simply the *mesiodistal* (resp. *buccolingual*) *line*.

We define the *cross-section* of (the mesh of) a tooth object with respect to a plane as the piecewise-linear curve obtained by intersecting the plane with the triangular faces of the mesh. A plane that is parallel to both L_{md} and the *z*-axis and intersects the tooth object generates a *mesiodistal cross-section*. Let P_{md} be a set of such uniformly-spaced planes and let the set of corresponding cross-sections generated be M. Similarly, a plane that is parallel to both L_{bl} and the *z*-axis and intersects the tooth object generates a *buccolingual cross-section*. Let P_{bl} be a set of such uniformly-spaced planes and let the set of corresponding cross-sections generated be B (see Figure 10).

(a) (b) (c)

Fig. 10: Examples of planar cross-sections on the tooth surface (shown in cyan): (a) Buccolingual cross-sections. (b) Mesiodistal cross-sections. (c) Buccolingual cross-section of a molar.

4.3 Computing 2D curvatures of cross-sections

For any point p on a planar curve C, the curvature at p can be defined as the reciprocal of the radius of the osculating circle at the point, which is the largest circle tangent to the curve on the concave side of p [10]. The 2D curvature of C at p can also be defined as the rate of change, at p, of the angle between the tangent vector to the curve at p and the positive *x*-axis [10]. It measures how sharply the tangent to C rotates at the given point. Thus, the curvature at point p of the curve shown in Figure 11 can be defined as,

$$\kappa(p) = \lim_{\Delta s \to 0} \frac{\Delta \theta}{2(\Delta s)} \tag{1}$$

where Δs is a small length along the curve and $\Delta\theta$ is the angle between the tangents at points $p+\Delta s$ and $p-\Delta s$ along the curve.

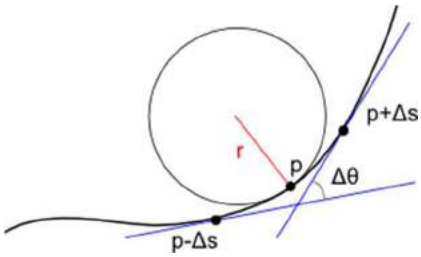

Fig. 11: Curvature of point p on a planar curve is defined rate of change, at p of the angle between the tangent vector to the curve at p and the positive x-axis. It is also defined as $1/r$, where r is the radius of the osculating circle at p (shown in red).

The curves in real-world applications may not have a reasonable analytical form and are often represented as a sequence of points sampled along the curve (Figure 12). Some examples of these are the contours in images, boundaries of shapes and, as in our case (Section 4.2), the intersection of a plane and a tooth surface. For these piecewise-linear curves, we have to approximate the curvature at its sampled points. A natural solution to this would be to first get a smooth spline approximation to the given curve followed by computing the curvature analytically using the first and second derivatives at each sampled point. However, this becomes an expensive operation for large numbers of points and as we need to compute the curvatures for a large number of curves, we need an alternative method to compute approximate curvatures efficiently.

In analogy with Equation 1, the approximate curvature of the point p_i (see Figure 12) on a planar curve can be evaluated as

$$\kappa(p_i) = \frac{\Delta\theta}{|p_{i-1}p_i| + |p_i p_{i+1}|} \tag{2}$$

where p_{i-1} (resp. p_{i+1}) is the previous (resp. next) point with respect to p_i on the curve C and $|p_i p_j|$ is the length of the edge from p_i to p_j. If the curve is not closed we define the curvatures to be zero at the start and the end. Also, we use the signed angle to define positive and negative curvatures at points. The points corresponding to the positive (resp. negative) curvatures form the convex (resp. concave) regions on the curve with respect to the plane containing the curve (Figure 10(c)).

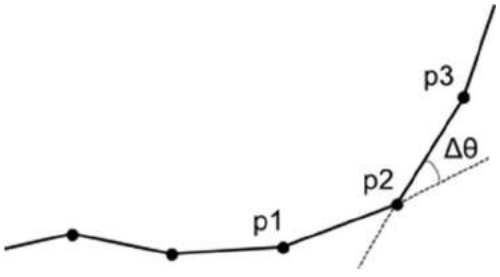

Fig. 12: Planar curve represented as a sequence of points.

4.4 Clustering of High Curvature Regions

Given the buccolingual and mesiodistal cross-sections of a tooth, we find the vertices on the curves for which the magnitude of the 2D curvature is greater than a specified threshold, T_{curv}. The sign of the curvature threshold may be positive or negative depending on the targeted feature (e.g., ridges (resp. grooves) have high positive (resp. negative) curvatures). The set, S, of high-curvature vertices resulting from the thresholding serves as the input to the clustering algorithm.

Our goal behind clustering is to aggregate the vertices in S into connected components of high-curvature vertices that correspond to features of interest. The extracted clusters reveal these features and also cause noise regions to be grouped into small isolated components. The latter can be identified and deleted easily using a threshold, T_{noise}, on the number of noise vertices.

We compute the connected components as follows. Initially all vertices in S are taken to be singleton components. Starting with this, we repeatedly merge a pair of components if the closest distance between them is less than a specified threshold, T_{ccd}. The closest distance between two components is defined as the minimum of the pairwise distances between their corresponding vertices.

The clustering method requires three user-specified threshold parameters: T_{curv}, T_{noise} and T_{ccd}.We have observed experimentally that, for each feature type of interest, values of these parameters can be found that work across a broad range of patient datasets. Thus, the parameter values can be predetermined and our algorithm does not, in general, require user input during routine operation. Section 5 below, which describes how the methods of this section can be used to identify various features, provides the specific parameter values that our implementation uses.

4.5 Discussion

The features of interest to us could be defined naturally in terms of the curvatures at the mesh vertices (relative to the underlying 3D surface) [6, 9, 14, 16, 22]. For example, cusps, incisal edges, and ridges consist of clusters of vertices of high positive curvature (convex regions), whereas grooves consist of clusters of vertices of high negative curvature (concave regions). Hence, it is natural to wonder if 3D curvature analysis can be used for feature recognition.

We implemented this approach and found that, unfortunately, it did not perform well on most datasets. There are several reasons for this:

- Tooth surfaces tend to exhibit sharp changes in curvature over small neighborhoods. This makes it difficult to compute 3D curvatures reliably and use them to identify partitioning ridges and valleys.
- For each feature type, the 3D curvature threshold settings vary quite considerably from one model to the next (in contrast to the situation in the 2D approach); this requires users to set the thresholds on a case-by-case basis and imposes an undue burden.
- The presence of spurious ridge- and groove-like structures on the occlusal surface and very close to the target features makes the identification and cleanup of actual features difficult. We tried using skeletonization methods for 3D meshes that are based on morphological operators [21], but these did not perform well given the nature of the problem. Moreover, as Figure 13 shows, the sizes of these noise regions are comparable to those of actual features, which makes identification of true features extremely difficult.

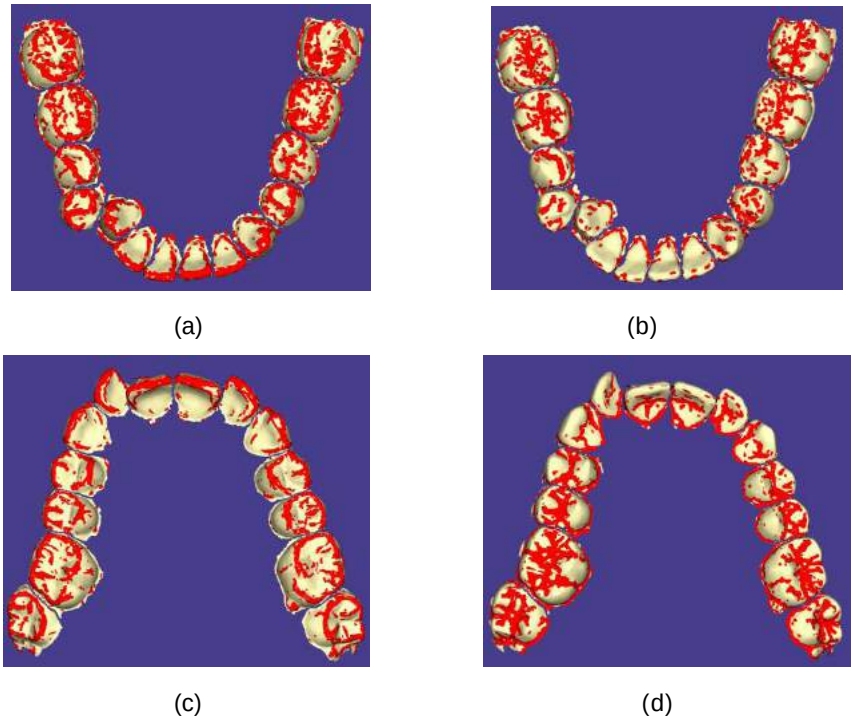

Fig. 13: Examples of poor feature recognition using 3D surface curvatures on a lower and an upper arch. The sizes of noise regions are comparable to those of actual features.

It is for these reasons that we chose to develop the 2D method, based on cross-sections, outlined earlier. It is easy to see that using a large number of cross-sections effectively reproduces the entire tooth surface to high accuracy. Since the cross-sections are generated by a set of parallel planes, this process can be thought of as a **ò**guided**ó** reconstruction of the 3D surface. An advantage of this is that we now have the flexibility to select only those parts of the cross-sections that yield interesting information. For example, on a buccolingual cross-section of a molar, the outermost convex regions corresponds to the mesial and distal cusp ridges and the innermost concave regions correspond to the grooves (Figure 10(c)). The notions of **ò**outermost**ó** and **ò**innermost**ó** are easy to define relative to the natural directionality provided by a 2D curve, but it is not clear how to do this on a surface. Furthermore, the parallel orientation of the cross-sections makes it easy to stitch together the portions of features found on each cross-section into a 3D feature.

5 FEATURE IDENTIFICATION

This section describes how the techniques of Section 4 can be used to automatically identify features other than cusps, such as incisal edges, grooves, marginal ridges, and occlusal surface boundary. (Cusp identification, via a different approach, was discussed in Section 3.) The purpose here is to provide the reader with a qualitative feel for how the proposed algorithms perform on real-world data, using sample meshes obtained from scanners such as *e*model [25] and 3Shape [26]. Quantitative validation results are given in Section 7.

5.1 Incisal Edges

These can be extracted as a cluster of vertices of high positive curvature (i.e., convex regions) on the buccolingual cross-sections of the anterior teeth. The results of our incisal edge detection algorithm are shown in Figure 14 for two pairs of upper and lower arches. Note that the algorithm performs correctly even when the tooth is in a rotated position from the global archform (Figures 14(b) and 14(d)).

As mentioned in Section 4.4, there are three parameters that control the clustering process. Their specific values for incisal edge identification are as follows: T_{curv}=0.6 (the curvatures are normalized to the range [-1,1] here and later), T_{noise}=1/10 of the number of buccolingual cross-sections and T_{ccd}=0.5 mm. (We reiterate that these parameters work well on all models tested here and later, and do not require adjustment by the user.)

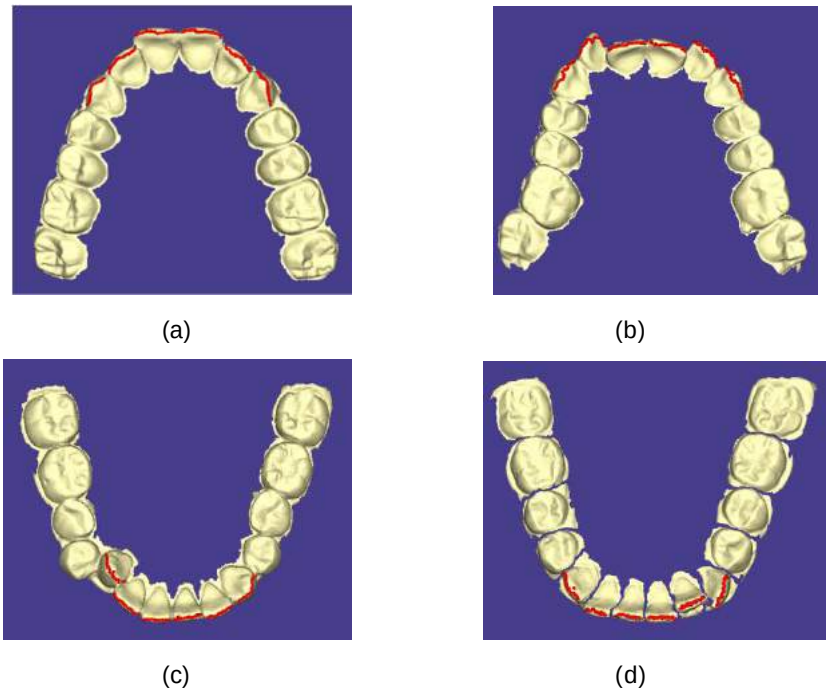

(a) (b) (c) (d)

Fig. 14: Incisal edges (shown red) on anteriors identified using buccolingual cross-sections. Upper arches shown in (a) and (b); lower arches in (c) and (d).

5.2 Grooves

Grooves are found on the posterior teeth and are extracted as a cluster of vertices of high negative curvature (i.e., concave regions) in the middle-section of the buccolingual cross-sections (Figure 10(c)). As mentioned in Section 2, there are many types of grooves on the posteriors, especially the molars. We are interested in the central grooves that run along the mesiodistal line of the tooth. Figure 15 shows the results of our groove identification algorithm on two pairs of upper and lower arches. As expected, the grooves on the upper arches have more variation than the ones on the lower arches and consist of multiple **ò**branches**ó**. For the purpose of treatment planning, one may choose to approximate these grooves by a straight line segment or a curve.

The specific parameter values used for groove identification are as follows: T_{curv}=-0.4, T_{noise}=1/10 of the number of buccolingual cross-sections and T_{ccd}=0.5 mm.

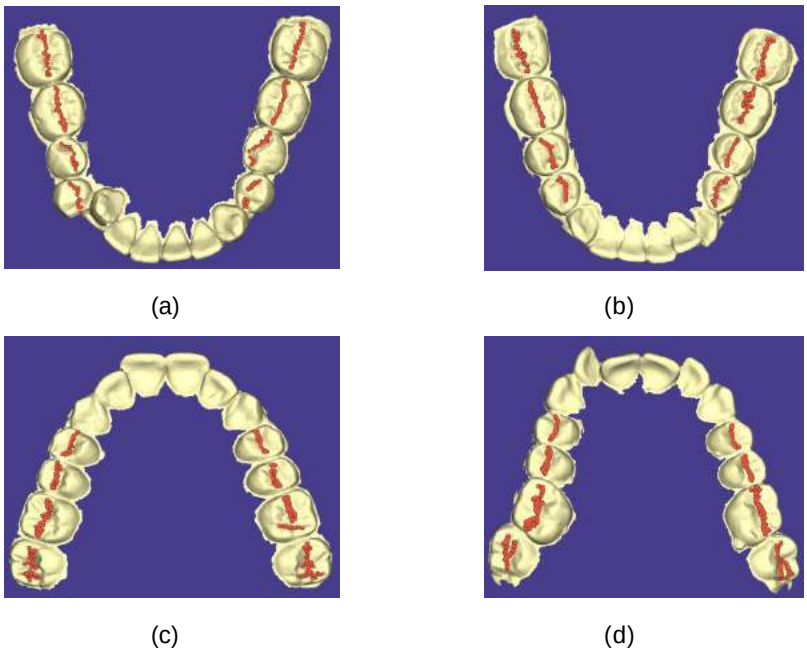

Fig. 15: Central grooves (shown brown) on posteriors identified using buccolingual cross-sections. Note the difference in the groove patterns between the lower arches ((a), (b)) and upper arches ((c), (d)).

5.3 Marginal Ridges

These are extracted as a cluster of vertices of high positive curvature on the mesiodistal cross-sections of the tooth surface. Figure 16 shows the results of our algorithm on two pairs of upper and lower arches. The marginal ridges on the lower arch premolars are difficult to identify because they are not easily separable from the cusp ridges and also may not be properly aligned with the mesiodistal line (see Figure 16(a) and (b)). Also, the distal marginal ridge on the last available molars often cannot be accurately identified because of the inherent ambiguities in the structure of these teeth.

The specific parameter values used for marginal ridge identification on an upper arch is T_{curv}=0.3, T_{noise}=1/10 of the number of mesiodistal cross-sections and T_{ccd}=0.5 mm. The mesial and distal walls on the lower arch posteriors are higher than those on the upper arch and, thus, we set T_{curv}=0.6. The threshold for T_{noise} and T_{ccd} are the same as for the upper arch.

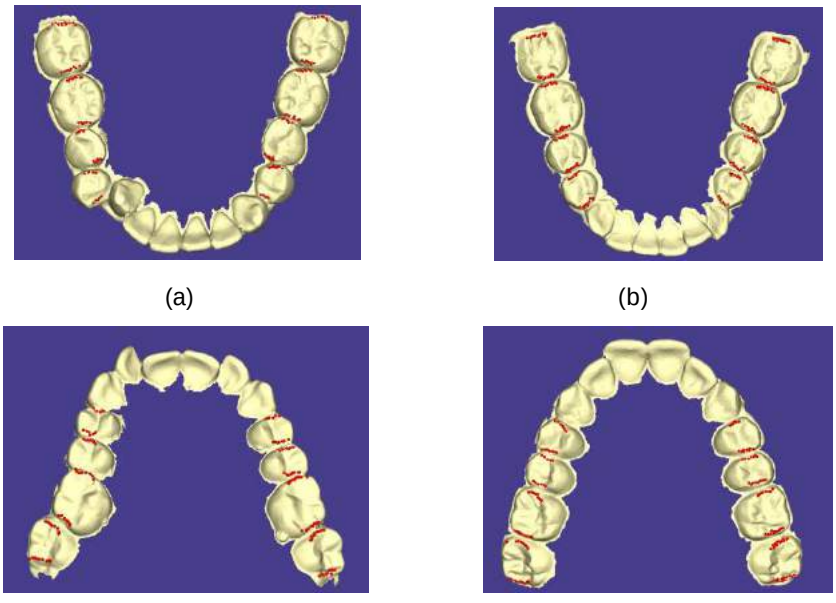

(a) (b)

(c) (d)

Fig. 16: Marginal ridges (shown red) identified on posterior teeth using mesiodistal cross-sections.

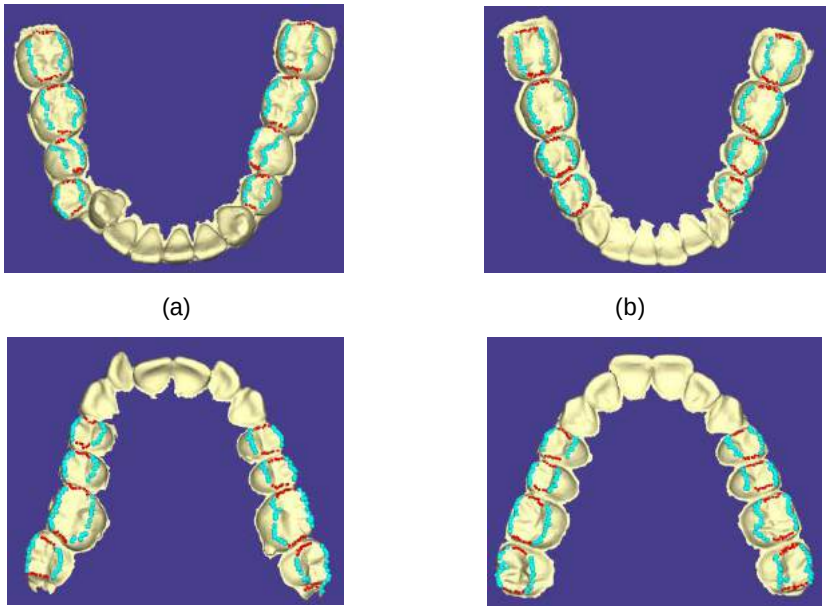

(a) (b)

(c) (d)

Fig. 17: Occlusal surface boundary identification on posterior teeth using buccolingual cross-sections. The occlusal surface is bounded by the marginal ridges found earlier (shown red) and the cusp ridges on the buccal and lingual sides (shown cyan).

5.4 Occlusal Surface Boundary

The occlusal surface boundary of a posterior tooth is defined by the marginal ridges on the mesial and distal sides, and the cusp ridges on the buccal and lingual sides (Section 2). Section 5.3 describes how to identify the marginal ridges. Cusp ridges on the buccal and lingual sides are also identified via buccolingual cross-sections, employing an approach similar to that for the incisal edges, but using both the buccal and the lingual sides of the cross-sections. Figure 17 shows the result of our cusp ridge identification algorithm.

The specific parameter values used for the cusp ridge identification are T_{curv}=0.5, T_{noise}=1/10 of the number of buccolingual cross-sections, and T_{ccd}=0.5 mm.

6 IDENTIFICATION OF DERIVED FEATURES

This section describes the estimation of derived features (archform and occlusal plane) from the already identified intrinsic features (cusps and incisal edges).

6.1 Archform

The archform is defined as an appropriate smooth curve through the incisal edges of anteriors, canine cusps, and the buccal cusps of molars and premolars. There have been several attempts to mathematically describe the archform, the most relevant ones being based on *catenary curves* [7], *cubic splines* [2, 5] and *beta functions* [3]. However, due to the large variation in the shape of the archform among humans with normal occlusion (square, tapered, ovoid, etc. [17]), it is difficult to formulate a single mathematical expression to describe all archforms.

Moreover, in most situations, an orthodontist is very likely to make a few minor changes to the archform during virtual treatment planning. Thus, our approach is to compute an initial approximation to the archform using the intrinsic features and allow the user to modify it using five control points along the archform curve (Figure 18).

We use the experimentally derived equation in [3] to compute the initial approximation to the archform as:

$$Y = 3.0314 \cdot D \cdot \left[\frac{1}{2} + \frac{X}{W}\right]^{0.8} \left[\frac{1}{2} - \frac{X}{W}\right]^{0.8} \tag{3}$$

where W is the distance between the distobuccal cusps of the first molars and D is the perpendicular distance between the line joining these cusps and the most anterior point between the two central incisors (this is computed as the midpoint between the incisal edges of central incisors). See Figure 18(a). We note that our definition of W follows common orthodontic practice and is slightly different than the one in [3], where W is measured as the distance between the distobuccal cusps of the second molars. This change is motivated by the fact that the second molars may not have completely erupted in many patients.

As mentioned above, our software interface provides five control points (Figure 18) to modify the archform. Once one of these control points is moved, the archform latches on to the five control points and is then computed as a cubic spline through these control points, which is another popular way to describe the archform in dental literature. (The control points can be moved symmetrically, in pairs or independent of one another.)

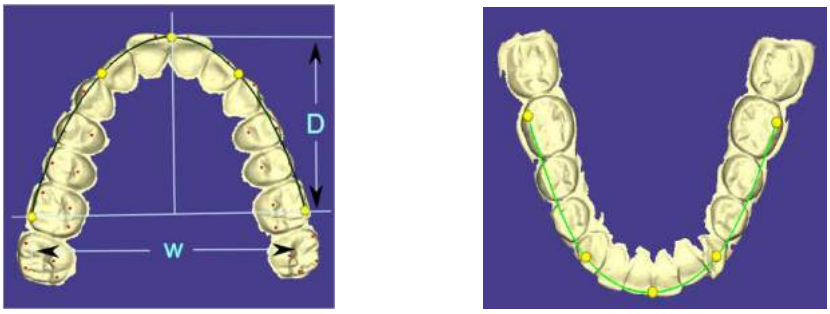

(a) (b)

Fig. 18: (a) An approximation to the dental archform (shown green) and the parameters of the beta function that describe it (shown as W and D). The archform can be modified using the five control points (shown yellow). (b) Archform of a lower arch.

6.2 Occlusal Plane

The occlusal surface is the surface of contact between teeth from opposing arches. Generally, even though the occlusal surface is not planar in normal-occlusion arches, a flat occlusal plane is set as the treatment goal in orthodontics [1]. This is based on a natural tendency of the teeth to rotate away from this plane (thus deepening the *curve of Spee*, which is a smooth curve connecting the posterior buccal cusps, canine cusps and the incisal edges on a single side of the arch [23]).

We approximate the occlusal surface as a plane through the mesiolingual cusps of the first molars and the midpoint of the incisal edges on the two central incisors (Figure 19). As in the case of the archform, a user may want to adjust the orientation and the height of the occlusal plane and we provide the required interface in our system to accomplish this.

(a) (b)

Fig. 19: Two views of the occlusal surface of an arch approximated as a plane through the mesiolingual cusps of the first molars and the midpoint of the central incisors (shown cyan).

7 EVALUATION

This section describes the software interface developed for evaluating the computed features and the results of the evaluation.

7.1 Setup

A software tool for feature identification was developed by us and was used for feature evaluation by an expert. The tool is written in C++ using Qt Open-Source Edition 4.5. It consists of a simple, intuitive user interface that can be used to load dental models and compute their features using the techniques described above. Figure 20 shows a screenshot of the tool. Note that the initial computation of features does not require any input from the user; however, a user can subsequently modify the computed features using buttons shown on the upper portion of the rightmost window in Figure 20.

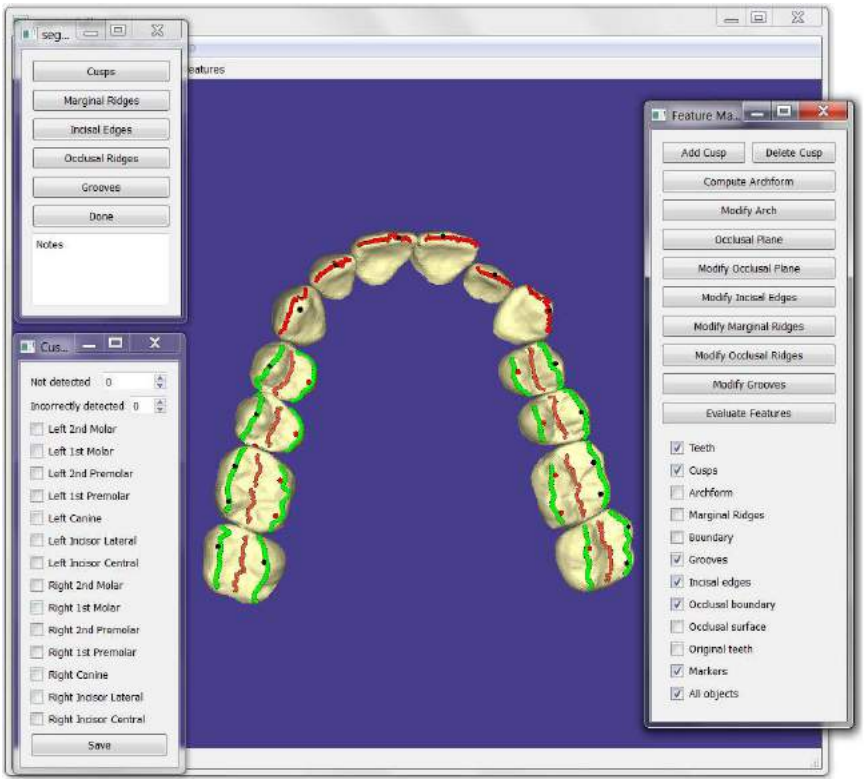

Fig. 20: Screenshot of the feature evaluation tool. A model is shown along with its computed features in the central window. The checkboxes on the rightmost window are used to show or hide the different feature types. Each button on the upper-left window, when clicked, selects a type of feature to be evaluated using the window shown on the lower-left side. The expert can record the number of errors corresponding to that feature type and specify the teeth contributing to the errors using the checkboxes. The expertôs input are recorded in a file for later analysis.

7.2 Results

The techniques for feature identification described in Sections 3 and 5 were evaluated on a set of 8 lower and 8 upper arches. These presegmented arches were selected from a database of actual cases treated at the University of Minnesota's dental clinic. The models were obtained through the SureSmile® software [24] which provides a large number of models of real-world cases that will be useful for the subsequent study of orthodontic alignment of teeth using the features computed here [13]. The validation models represented a reasonable sample of real-world variation in tooth size, shape and orientation and were selected from actual patients being treated. The models represent real dentitions with the associated anatomical variation. (Recall that qualitative results were given in Section 5, using meshes obtained from a different set of scanners, i.e., *e*model [25] and 3Shape [26].)

All the features identified by the algorithms described earlier were evaluated by an experienced orthodontist. The criteria for evaluation was the accuracy of the detected feature with respect to the anatomy of the corresponding tooth and its purpose in the orthodontic alignment planning. For example, often the lower molars may have 4 or 5 prominent cusps all which must be detected. On the other hand, often due to wear, some cusps may not be prominent enough on a tooth. Thus, these will not be included in the target set of cusps. Similar issues exist with other features as well.

The errors in features were classified into three categories: partially detected (e.g., only a portion of a ridge was identified), incorrectly detected (the feature was found in an incorrect part of a tooth) and missing (feature was not identified at all, e.g., an unidentified cusp). The aggregated results of the evaluation on the 16 input arches are shown in Table 1.

Feature Type	Partial	Incorrect	Missing	Correct	Total	% Correct
Cusps	3	3	23	383	412	92.9
Marginal ridges	8	6	1	241	256	94.1
Cusp ridges	8	5	0	243	256	94.9
Incisal edges	2	0	0	94	96	97.9
Grooves	1	1	0	126	128	98.4

Tab. 1: Aggregated results of the evaluation of features on 16 different dental arches.

Incisal edges and grooves: The identification of incisal edges and grooves is extremely accurate as seen in the last two rows of Table 1. Each arch had 6 incisal edges (4 incisors and 2 canines) and 8 grooves (4 posterior teeth on both left and right sides). The difficulty in incisal edge identification is primarily due to malocclusions and tooth wear on the incisors. Similarly, groove identification is sometimes difficult due to irregular anatomy and tooth wear. Also, we are interested in approximating the central grooves on the posteriors (along the mesio-distal axis), which are quite curved on the lower premolars and the upper molars.

Cusps: Table 1 shows the results of cusp identification. The number of true cusps varies across different arches, and the majority of errors is due to unidentified cusps on second molars (Figure 21(a)). This is primarily due to incorrect orientation and insufficient anatomical details. It was observed that more than half of these errors came from only three different arches.

Occlusal surface boundary: Table 1 shows the results for identification of marginal and cusp ridges which constitute the occlusal surface boundary. Each arch has 8 posterior teeth with 2 marginal and 2 cusp ridges. As with the other features, it is observed that most of the errors are from the second molars due to similar reasons (Figure 21(b) and 21(c)).

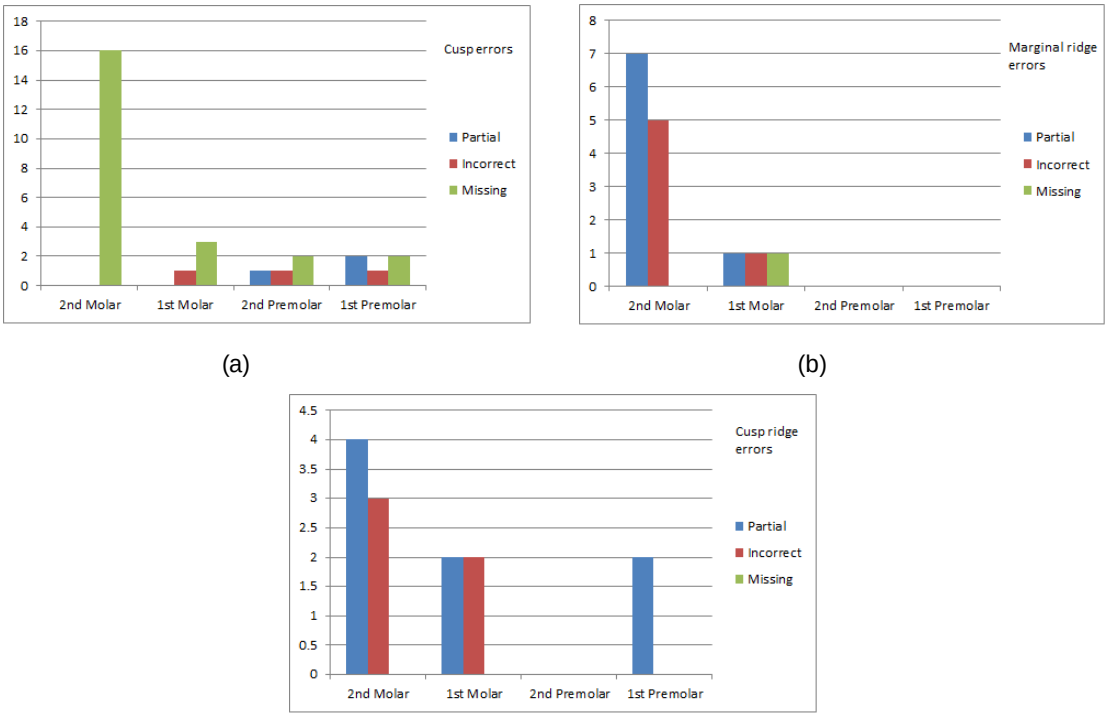

Fig. 21: These charts show the errors in feature identification with respect to the different tooth types shown on the -axis): (a) Errors in cusps, (b) Errors in marginal ridges, and (c) Errors in cusp ridges.

8 CONCLUSION

We have presented techniques to automatically identify tooth surface features in noisy and incomplete dental mesh models. These features are important in virtual orthodontic treatment planning. Our methods use buccolingual and mesiodistal cross-sections of the tooth surface to facilitate a **ò**guided**ó** extraction of incisal edges, central grooves, marginal ridges, cusp ridges, and occlusal surface boundary. We also described a watershed-based cusp identification algorithm. The algorithms have been implemented and experiments on real-world datasets show that the methods are effective in automatic feature identification.

ACKNOWLEDGMENT

This research was supported, in part, by the Orthodontics Education and Research Fund at the University of Minnesota. The authors thank the three reviewers for their helpful comments.

REFERENCES

[1] Andrews, L. F.: The six keys to normal occlusion, *Am. J. Orthod.*, 62(3), 1972, 296ð309. http://dx.doi.org/10.1016/S0002-9416(72)90268-0

[2] Begole, E. A.: Application of the cubic spline function in the description of dental arch form, *J. Dent. Res.*, 59(9), 1980, 1549ð1556. http://dx.doi.org/10.1177/00220345800590092901

[3] Braun, S.; Hnat, W. P.; Fender, D. E.: The form of the human dental arch, *Angle Orthod.*, 68, 1998, 29ð36.

[4] Chang, Y.; Xia, J. J.; Gateno, J.; Xiong, Z.; Zhou, X.; Wong, S. T. C.: An automatic and robust algorithm of reestablishment of digital dental occlusion, *IEEE Trans. on Medical Imaging*, 29(9), 2010, 1652ð1663. http://dx.doi.org/10.1109/TMI.2010.2049526

[5] Diggs, D. B.: *The quantification of arch form*. Ph.D. thesis, University of Washington, 1962.

[6] Gatzke, T.; Grimm, C. M.: Estimating curvature on triangular meshes, *Intl. J. of Shape Modeling*, 12(1), 2006, 1ð28. http://dx.doi.org/10.1142/S0218654306000810

[7] Germane, N.; Lindauer, S. J.; Rubenstein, L. K.; Revere Jr, J. J.; Isaacson, R. J.; Increase in arch perimeter due to orthodontic expansion, *Am. J. Orthod. Dentofacial Orthop.*, 100(5), 1991, 421ð427. http://dx.doi.org/10.1016/0889-5406(91)70081-7

[8] Hiew, L. T.; Ong, S. H.; Foong, K. W. C.: Optimal occlusion of teeth using planar structure information, *Mach. Vision Appl.*, 21(5), 2010, 735ð747. http://dx.doi.org/10.1007/s00138-009-0191-1

[9] Hoffman, D. D.; Singh, M.: Salience of visual parts, *Cognition*, 63(1), 1997, 29ð78. http://dx.doi.org/10.1016/S0010-0277(96)00791-3

[10] Klette, R.; Rosenfeld, A.: *Digital geometry*, Morgan Kaufman, 2004.

[11] Kronfeld, T.; Brunner, D.; Brunnett, G.: Snake-based segmentation of teeth from virtual dental casts, *Comp.-Aided Design. and Appl.*, 7(2), 2010, 221ð233.

[12] Kumar, Y.; Janardan, R.; Larson, B.; Moon, J.: Improved segmentation of teeth in dental models, *Comp.-Aided Design. and Appl.*, 8(2), 2011, 211ð224.

[13] Kumar, Y.; Janardan, R.; Larson, B.; Moon, J.: Automatic virtual alignment of dental arches in orthodontics, Manuscript in preparation, 2012.

[14] Lee, Y.; Lee, S.; Shamir, A.; Cohen-Or, D.; Seidel, H.: Intelligent mesh scissoring using 3D snakes, In *Proc. Comp. Graphics and Appl.*, 2004, 279ð287.

[15] Mangan, A. P.; Whitaker, R. T.: Partitioning 3D surface meshes using watershed segmentation, *IEEE Trans. on Vis. and Comp. Graphics*, 5(4), 1999, 308ð321.

[16] Meyer, M.; Desbrun, M.; Schröder, P.; Barr, A.: Discrete differential geometry operators for triangulated 2-manifolds, *VisMath.*, 2002, 35ð54.

[17] Noroozi, H.; Nik, T. H.; R. Saeeda, R.: The dental arch form revisited, *Angle Orthod.*, 71, 2001, 386ð389.

[18] American Board of Orthodontics. Grading system for dental casts and panoramic radiographs, 2010, http://tinyurl.com/ygstyfu.

[19] Page, D. L.; Koschan, A. F.; Abidi, M. A.: Perception-based 3D triangle mesh segmentation using fast marching watersheds, In *CVPR '03: Proc. of the Intl. Conf. on Computer Vision and Pattern Recognition*, 2003, 27ð32.

[20] Pulla, S.; Razdan, A.; Farin, G.; Improved curvature estimation for watershed segmentation of 3-dimensional meshes. Manuscript, 2001.

[21] Rössl, C.; Kobbelt, L.; Seidel, H.; Stadtwald, I.: Extraction of feature lines on triangulated surfaces using morphological operators, *AAAI Symp. on Smart Graphics*, 2000, 71ð75.
[22] Weinkauf, T.; Günther, D.: Separatrix persistence: Extraction of salient edges on surfaces using topological methods. *Computer Graphics Forum (Proc. SGP '09)*, 28(5), 2009, 1519ð1528.
[23] Woelfel, J. B.; Scheid, R. C.: *Dental Anatomy: Its Relevance to Dentistry*, Lippincott Williams & Wilkins, 2011.
[24] SureSmile®. http://www.suresmile.com/.
[25] *e*model®8.5. http://www.geodigmcorp.com.
[26] 3Shape OrthoAnalyzer Software™. http://tinyurl.com/d26agep.